Comprehensive analysis of immune ferropotosis gene on renal clear cell carcinoma: Prognosis and influence of tumor microenvironment

Lin-hui Yang
Fujian Provincial Hospital, Shengli Clinical Medical College of Fujian Medical University
Li-zhen Xu
Fujian Provincial Hospital, Shengli Clinical Medical College of Fujian Medical University
Zhi-jian Huang
Fujian Medical University Cancer Hospital, Fujian Cancer Hospital
Hong-hong Pan
Fujian Provincial Hospital, Shengli Clinical Medical College of Fujian Medical University
Min Wu
Fujian Provincial Hospital, Shengli Clinical Medical College of Fujian Medical University
Qiu-yan Wu
Fujian Provincial Hospital, Shengli Clinical Medical College of Fujian Medical University
Tao Lu
Fujian Provincial Hospital, Shengli Clinical Medical College of Fujian Medical University
Yan-ping Zhang
Fujian Provincial Hospital, Shengli Clinical Medical College of Fujian Medical University
Yao-bin Zhu
Fujian Medical University
Jia-bin Wu
Fujian Provincial Hospital, Shengli Clinical Medical College of Fujian Medical University
Jie-wei Luo
Fujian Provincial Hospital, Shengli Clinical Medical College of Fujian Medical University
lie-fu Ye (yeliefu@126.com)
Fujian Provincial Hospital, Shengli Clinical Medical College of Fujian Medical University

Research Article

Keywords: immunity, ferropotosis, renal clear cell carcinoma, prognosis, biomarker

Posted Date: May 9th, 2022

DOI: https://doi.org/10.21203/rs.3.rs-1611057/v1

Abstract

In this study, immune-ferropotosis-related prognostic differentially expressed genes (IFR-DEGs) were selected from the TCGA database, and a total of 103 differentially expressed genes were found. Fifty-two differentially expressed genes related to immunity and ferropotosis were identified using univariate Cox analysis. Stepwise regression was used to establish a Lasso-Cox risk score prognostic model consisting of four immune ferropotosis genes, and overall survival (OS) was significantly better in low-risk patients than in high-risk patients (training set: $P < 0.001$).In multivariate Cox regression analysis, the risk score was an independent predictor of OS ($HR > 1$, $P < 0.001$). Time-dependent ROC curve analysis indicates that the model has good predictive ability. The prognostic model was also well validated in the validation set and the total TCGA cohort. Subcellular fluorescence localization of model genes showed that ACADSB, CHAC1, and PLA2G6 were distributed in the cytoplasm, while LURAP1L was distributed in the nucleus. The expression of mRNA and protein suggested that ACADSB and CHAC1 were lower in renal carcinoma than in normal renal tissue, LURAP1L and PLA2G6 were higher in renal carcinoma. RNA sequencing localization analysis of ACADSB single-cell indicated that ACADSB was enriched in the distal tubule cluster. After mutation correlation analysis of model genes, 1.56% (7/448) patients were found to have genetic changes, ACADSB was significantly positively correlated with LURAP1L, and negatively correlated with CHAC1 and PLA2G6. CHAC1 was negatively correlated with LURAP1L. We found that CD8+T cells, regulatory T cells (Tregs), macrophage M0, and macrophage M1 levels were significantly higher in high-risk than low-risk patients. Among immune-related functions, we also found that the high-risk group had higher immune function in terms of immune checkpoint, proinflammatory, T-cell co-inhibition, and type II interferon response. Compared with the low-risk group, the high-risk group had a higher immune score in the immune microenvironment, a stronger immune escape ability, and a higher abundance of immune checkpoints. A novel prognostic model of immune ferropotosis-related genes (ACADSB, CHAC1, LURAP1L, and PLA2G6) was constructed, which can effectively predict the survival of patients with KIRC and play an important role in immune infiltration, microenvironment, and immune escape.

1 Introduction

Renal cell carcinoma (RCC), the most common type of kidney cancer, is believed to originate from renal epithelial cells, affecting over 400,000 people worldwide annually[1]. RCC is divided into three main histological subtypes: clear cell RCC (KIRC), papillary cell RCC (pRCC or KIRP), and chromophobe cell RCC (chRCC). KIRC is the most common pathological type of adult renal cell carcinoma and accounts for over 80% of all clinical cases[2]. Most local KIRC can be ablated by partial or radical nephrectomy[3] or active monitoring[4]. For advanced or metastatic kidney cancer, many new therapies have emerged over the past 20 years, including vascular endothelial growth factor inhibitors and tyrosine kinase inhibitors, most of which have achieved good results. The etiology of KIRC is complex, and the tumor tissue is highly heterogeneous, and because the kidneys are hidden in the body, many patients have no symptoms of kidney cancer when it reaches an advanced stage[5]. At the time of diagnosis, 30% of patients are diagnosed with distant metastases[6]. Although local RCC can be cured by surgical resection, approximately 40% of surgical patients eventually relapse, which has led to only small improvements in

KIRC outcomes over the past two decades[7]. The diagnosis and treatment of patients remains poor, and thus the study of the mechanism of KIRC is of great significance to improve the prognosis of patients.

There is growing evidence that the immune system plays a role in cancer[8]. The tumor immune microenvironment (TIME) is a cellular immune ecosystem composed of immune cells, the extracellular matrix, fibroblasts, endothelial cells, and various cytokines, which are closely related to the occurrence and development of tumors[9, 10]. For example, various immune cells, including CD8 + T cells, CD4 + T cells, and NK cells, have been associated with KIRC tumors[11]. In recent years, it has been found that the prognosis of renal clear cell carcinoma is not only related to the pathological stage, but also that the tumor immune status may have an important influence on the prognosis of patients[12]. In recent decades, with the development of immunotherapy, tumor therapy has undergone revolutionary changes, with immunotherapy considered a promising therapeutic field[13]. Researchers have found that the immune microenvironment can serve as an important prognostic indicator, which could also improve the potential for precision therapy[14]. The analysis of the immune microenvironment will help improve the response to immunotherapy, wherein an in-depth understanding of TIME is essential to identify potential immunotherapeutic targets for RCC. In a sense, all tumors are immunogenic. The host immune system generates a T-cell response that recognizes and kills cancer cells[15]. A large number of studies have shown that KIRC is highly immunogenic[16] and that the existence of immune detection points allows tumor immune escape[17]. Therefore, immune checkpoint blockade (ICB) is a novel therapeutic strategy that has been used in many cancer types[18–21]. The treatment of renal cell carcinoma has also made rapid progress. In conclusion, with the successful application of immune checkpoint inhibitors (ICIs), tyrosine kinase inhibitors (TKI) and vascular endothelial growth factor (VEGF) targeting drugs, it plays an important role in the individualized and comprehensive treatment of patients with renal cell carcinoma, especially metastatic renal cell carcinoma.[22]

Ferroptosis is a novel type of cell death characterized by iron-dependent cell death and superoxide lipid accumulation, with genetic, biochemical, and morphological characteristics[23]. The dysfunction of the cellular antioxidant GPX4 is known to contribute to ferropotosis process. GPX4 synthesis depends on intracellular cystine transported by the xCT system[24]. The solute carrier family of seven members 11 (SLC7A11) constitutes a major component of the xCT system and can inhibit ferropotosis by promoting cysteine uptake. Increasing evidence shows that ferropotosis is closely related to various physiological and pathological states of the human body[24, 25]. Ferropotosis is also closely related to the occurrence and development of tumors. Studies have shown that ferropotosis-related factors or pathways can regulate the sensitivity of tumor cells to ferropotosis by affecting iron metabolism, ROS synthesis, antioxidant systems, and other related mechanisms. This suggests that SLC7A11, which is overexpressed in a variety of cancers, can promote tumor progression by delaying ferropotosis, leading to metabolic reprogramming.[26]. It has been reported that ferritin phagocytosis is mediated by interaction with surface arginine residues in ferritin heavy chain 1(FTH1)[27, 28]. NCOA4 overexpression induces ferropotosis by increasing the intracellular free iron content, glutathione production, and reactive oxygen species (ROS) levels[29]. As ferropotosis plays a key role in a variety of diseases, including kidney cancer, targeting ferropotosis may be a potential treatment strategy for patients with KIRC.

A close relationship exists between tumor immunity and ferropotosis[30, 31]. Tumor-associated macrophages (TAM) are the main source of iron for tumor growth and release large amounts of iron into the tumor microenvironment[32]. Many studies on the relationship between immunity and ferropotosis have provided a new understanding of the pathogenesis of renal clear cell carcinoma, and ferropotosis intervention can effectively improve immunosuppression[33, 34]. Owing to the close relationship between immune and ferropotosis-related genes and tumors, the expression of immune ferropotosis-related genes in tumor tissues can be used to predict the prognosis of patients.

In this study, by analyzing the expression of the KIRC gene in the TCGA database and comparing it with the expression of genes related to immune ferropotosis at different levels, a prognostic model containing multiple genes was established, which can effectively predict the survival of patients with KIRC. By studying the relationship between the immune microenvironment and risk score, a potential mechanism is discussed and drug sensitivity was predicted, providing a basis for the clinical diagnosis and treatment of cancers, as well as a novel direction for the identification of therapeutic targets.

2 Results

A total of 530 patients with pathologically confirmed KIRC from the TCGA cohort were included in this study and randomly divided equally into two groups: 265 patients were included in the training set and 265 patients were included in the validation set.

2.1 Determination of DEGs related to prognosis of immune-ferropotosis

According to the gene expression data of TCGA patients, 6534 differential genes were obtained through differential analysis, and volcano maps were drawn according to the level of differential expression (Fig. 1a). Genes related to immunity and ferropotosis were intersected using a Venn diagram (Fig. 1b), and 103 intersected genes were obtained. Univariate Cox analysis was performed on genes related to immunity and ferropotosis. According to statistical significance ($P < 0.05$), 52 genes related to immunity and ferropotosis were obtained, from which forest maps were created: 23 low-risk genes and 29 high-risk genes (Fig. 1c).

2.2 Construction of immune-ferropotosis gene marker prognostic model (IFRSig)

Lasso-Cox regression was performed on prognostic genes using the GLNMET package in R to screen for the best prognostic genes. The Cox multivariate regression analysis coefficients of the prognostic genes were extracted (Fig. 1d and 1e). Risk scores were calculated based on gene expression levels using the following formula: Risk score= ∑(Expi × β I), where “Expi” denotes the gene expression level and β I represents the Cox risk ratio coefficient of genes. The risk score of this model was calculated as follows:

-0.578*ACADSB + 0.287*CHAC1-0.397*LURAP1L + 0.447*PLA2G6.

According to the median risk score of the TCGA cohort, the patients were divided into a high-risk group and low-risk group, then randomly divided into training set, validation set, and cohort at a ratio of 1:1 for verification.

To intuitively analyze the high- and low-risk groups, we adopted PCA and t-SNE technology, with dimension reduction as a two-dimensional plane, according to the dangerous degree of the median value of PCA and t-SNE image processing. According to the visualization images, most patients could be divided into high- and low-risk groups, and only a minority of patients could not be classified. This indicates that the model had a high sensitivity (Fig. 1f and 1g).

2.3 Validation of prognostic models

In the training set, high-risk patients had significantly lower survival rates than low-risk patients (Fig. 2a, d). This result was confirmed in the validation set and cohort (Fig. 2b-f). Heat maps were constructed to show the expression levels of the four prognostic genes in the high- and low-risk groups in the three cohorts (Fig. 2g-i).

Further survival analysis showed that the OS of high-risk patients in the training set was significantly lower than that in the low-risk group (Fig. 2j, $P < 0.001$), which was confirmed by the validation set and cohort (Fig. 2l and 2n, $P < 0.001$).The predictive ability of the risk score on OS was evaluated using time-dependent ROC curve analysis. The results showed that the AUC of the training set cohort were 0.802 (1 year), 0.746 (3 years), and 0.752 (5 years) (Fig. 2k), while the AUC of the verification set cohort were 0.696 (1 year), 0.699 (3 years), and 0.726 (5 years) (Fig. 2m). The AUC of TCGA cohort was 0.750 (1 year), 0.726 (3 years), and 0.736 (5 years) (Fig. 2o), suggesting that the model had good predictive ability.

2.4 Independent prognostic analysis of risk scores

To verify whether the risk score was independent of other prognostic factors, univariate and multivariate Cox proportional risk regression analyses were performed in the training set, validation set, and cohort, respectively. Univariate and multivariate Cox regression analyses were performed for age, sex, tumor stage, grade, and risk score, as shown in Fig. 3. The risk score and tumor stage of the training set, validation set, and total TCGA cohort were found to be significantly associated with OS, suggesting that tumor stage and risk score were independent predictors of OS (training set: HR = 1.313, 95%CI: 1.154–1.493, $P < 0.001$; validation set: HR = 1.178, 95%CI: 1.065–1.303, $P < 0.001$); total TCGA cohort: HR = 1.229, 95%CI: 1.140–1.326, $P < 0.001$).

2.5 Construction of the prediction column chart

To predict the survival probability of patients with KIRC, 1-, 3-, and 5-year nomograph were established in the cohort based on the prediction model (risk score) and clinical factors (T, N, and M) (Fig. 3g). According to the scoring results of each factor, the total value of the line graph can be obtained from the sum of the single scores of each factor associated with the overall score, which was used to estimate patient survival at 1, 3, and 5 years. To test the predictive power of the prognostic model of the nomograph, the calibration curve was used to evaluate the predictive model. The calibration curve was approximately 45 degrees,

acting as the base line (Fig. 3h), indicating a high consistency between the actual and expected survival rates of the model.

2.6 The high-risk group was closely associated with poor prognosis in patients with KIRC

To further evaluate the predictive power of the model, we re-assigned age, gender, G1-2, G3-4, T1-2, T3-4, M0, M1, N0, N1-3, Stage I-II, and Stage III-IV as prognostic and clinicopathological factors in KIRC patients in the TCGA cohort according to different conditions. In multiple clinical subgroups, age ≤ 65 ($P < 0.001$), age > 65($P < 0.001$), female ($P < 0.001$), male ($P = 0.007$), T1-2 ($P = 0.009$), T3-4 ($P < 0.001$), M0 ($P < 0.001$), M1 ($P = 0.008$), N0 ($P < 0.001$), N1-3 ($P = 0.866$), Stage I-II ($P = 0.016$), and Stage III-IV ($P < 0.001$) were indicative of the relationship between a high risk score and prognosis. We found that the Kaplan-Meier survival analysis and survival rate of each subgroup showed that regardless of age and gender, TM Stage and Stage, the survival time of patients in the low-risk prognostic model group was significantly prolonged, except that the high-risk prognostic curve in the N1-3 subgroup was insignificant. This suggests that the prognostic model has good predictive power in most subclinical subgroups (Fig. 4).

2.7 Enrichment analysis of functional pathways of DEGs

To elucidate why the model differentiated high- and low-risk patients with KIRC, the gene enrichment in high- and low-risk patients with KIRC was further compared. Using GO analysis, the differential genes were found to be enriched in biological process (BP), cell component (CC), and molecular function (MF) (Fig. 5a, Table 2). Differential genes were mainly enriched in complement activation (classical pathway) and complement activation of humoral immune response mediated by circulating immunoglobulins. Differential genes were mainly enriched in immunoglobulin complex, circulating immunoglobulin complex, blood particles, and other functions. In MF, the differential genes were mainly enriched in antigen binding, immunoglobulin receptor binding, chemokine activity, and other functions. In KEGG enrichment analysis, the differential genes were enriched in viral protein and cytokine and cytokine receptor interaction, cytokine-cytokine receptor interaction, PPAR signaling pathway, and other pathways. In GSEA analysis (Fig. 5b), the high-risk group showed abundant gene enrichment in diseases, immune system, innate immune system, hemostasis, and infectious diseases ($P < 0.05$). These results indicate that these functions and pathways were closely related to the development of KIRC.

2.8 Clinically relevant heat map

To observe the expression of prognostic model genes in clinical features, we constructed an expression heat map based on the correlation of clinical features to observe the expression relationship between the prognostic model genes in high- and low-risk groups, as well as patient age, sex, metastasis, tumor stage, grade, and immune score (Fig. 5c).

2.9 Expression and immunofluorescence localization of model genes in KIRC

According to the median value of gene expression in the prognostic model, patients with TCGA renal clear cell carcinoma data were divided into high- and low-expression groups. The mRNA expression levels of ACADSB and CHAC1 in renal clear cell carcinoma tissues were significantly lower than those in normal tissues (Fig. 6a-b). The mRNA expression levels of LURAP1L and PLA2G6 were significantly higher than those in the normal tissues (Fig. 6c-d). To investigate the subcellular localization of ACADSB, CHAC1, LURAP1L, and PLA2G6 in cancer cells, we used the HPA database to evaluate the distribution of ACADSB, CHAC1, LURAP1L, and PLA2G6 in renal tissue. As shown in Fig. 6e-h ACADSB and CHAC1 were mainly distributed in the mitochondria of U-2OS cells, while LURAP1L was mainly distributed in the nucleoli of A-431 cells. PLA2G6 was mainly distributed in the cytoplasm of the central line satellite of U-2OS cells.

In the TCGA-KIRC cohort, ACADSB and CHAC1 were low in renal clear cell carcinoma, whereas LURAP1L and PLA2G6 were higher in RENAL clear cell carcinoma than in adjacent non-tumor renal tissue. To confirm the expression of these four genes in clinical samples, we further validated the expression of proteins encoded by the four model genes using clinical samples from HPA. Immunohistochemical images of four gene signatures in normal kidney tissue and renal carcinoma are shown in Fig. 6i-p.

2.10 Single-cell RNA sequencing localization analysis of ACADSB gene

To evaluate the localization of model genes in single cells, we used the PanglaoDB dataset for single-cell RNA sequencing localization analysis; however, only ACADSB was found to be included in renal tissues. Therefore, we conducted ACADSB single-cell RNA sequence localization analysis. As shown in Fig. 6q and 6r, renal tissue cells were divided into eight cell clusters: distal tubule cells (P = 5.647E-14), endothelial cells (P = 1.14415E-19), macrophages (P = 1.38073E-10), podocytes (P = 5.62787E-05), main cells (P = 3.46711E-30), proximal tubule cells (P = 7.06537E-35), smooth muscle cells (P = 1.31683E-23), and unknown (P = 0.000803306). ACADSB was set as the superimposed expression of genes, and according to single-cell analysis, ACADSB was found to be enriched in clusters of distal tubule cells (Fig. 6s). This suggests that a decreased expression of ACADSB in the distal tubules plays an important role in the carcinogenesis of KIRC.

2.11 Mutation and correlation analysis of four model genes

To evaluate the mutation of four model genes in KIRC, we used cBioPortal database for data analysis. A total of 1.56% (7/448) of the patients were found to have genetic changes. Genetic changes in ACADSB included depth loss and splicing mutation, while genetic changes in CHAC1 included deep deletions. Similarly, genetic changes in LURAP1L included non-frameshift mutation and missense mutation, while genetic changes in PLA2G6 included missense mutations (Fig. 7a-b). Thereafter, Spearman correlation analysis was used to examine the correlation between model genes. As shown in Fig. 7c, ACADSB was significantly positively correlated with LURAP1L, and negatively correlated with CHAC1 and PLA2G6. CHAC1 was negatively correlated with LURAP1L.

2.12 Correlation between the model and immune cell infiltration

To better investigate the complex cross-talk between the prognostic model and immune characteristics, we evaluated the immune infiltrate profiles of 22 immune cells in clear renal cell carcinoma tissues between the high- and low-risk groups in the KIRC sample using the CIBERSORT algorithm (data visualized in a violin plot). The results showed that CD8 + T cells ($P < 0.001$), follicular helper T cells ($P < 0.01$), regulatory T cells (Tregs) ($P < 0.001$), activated NK cells ($P = 0.011$), and macrophage M0 ($P = 0.01$) were significantly increased in the high-risk group of KIRC patients. By contrast, monocytes ($P < 0.001$), macrophage M1 ($P < 0.001$), and macrophage M2 ($P < 0.001$) were significantly reduced in the high-risk group of KIRC patients (Fig. 7d).

2.13 Correlation analysis between risk score and immune cell abundance

With regards to the correlation between the risk score and immune cell abundance, Spearman correlation analysis showed that risk score was positively correlated with regulatory T cells (Tregs), macrophages M0, activated NK cells, plasma cells, CD8 + T cells, and follicular helper T cells (Fig. 7e-t). Risk scores were negatively correlated with naive B cells, active dendritic cells, resting dendritic cells, eosinophils, macrophages M1, macrophages M2, monocytes, neutrophils, resting mast cells, and resting memory CD4 + T cells (Fig. 7e-t).

2.14 Correlation of immune cells

Thereafter, the correlation of these 22 different immune cells was explored, and the results showed that Treg cells were positively correlated with CD8 + T cells and follicular helper T cells. CD8 + T cells were positively correlated with follicular helper T cells and T cells γδ. B cell infantile was positively correlated with plasma cell. Activated dendritic cells were positively correlated with eosinophils. Macrophage M2 was negatively correlated with CD8 + T cells and follicular helper T cells. The resting CD4 memory T cells were negatively correlated with CD8 + T cells and follicular helper T cells (Fig. 8a).

2.15 Risk score and immune-related function

Based on ssGSEA, the correlations between the risk scores and immune-related functions were determined, as shown in the boxplot in Fig. 8b. As a result, the high-risk group was found to have better immune function in terms of immune checkpoint activity, cytolysis activity, proinflammatory activity, T cell co-inhibition, and type II interferon response.

2.16 Kaplan-Meier survival analysis of immune cells

Subsequently, Kaplan-Meier survival analysis of immune cells was performed. The results showed that Treg cells, CD4 + T memory cells, follicular helper T cells, monocytes, inactive mast cells, and resting dendritic cells had a good predictive ability for OS (Fig. 8c-h).

2.17 Immune microenvironment and immune escape

To explore the relationship between the tumor microenvironment (TME), we performed TME scores and found that high-risk patients had higher immune scores and higher ESTIMATE scores than low-risk patients (Fig. 9a-c).To assess the potential of risk scores as biomarkers for immunotherapy or chemotherapy, we used the TIDE online tool to predict responses to immunotherapy in different risk groups. The TIDE score was found to be negatively correlated with the efficacy of immunotherapy, and the results showed that TIDE score of high-risk patients significantly increased ($P < 0.05$) (Fig. 9d-f), suggesting that the efficacy of immunotherapy in the high-risk group was worse than that in the low-risk group.

2.18 Immune checkpoints

Based on the importance of immunotherapy with checkpoint inhibitors, we further investigated the expression of immune checkpoints in both risk groups. The results showed that most immune checkpoints were more active in high-risk populations. The expression of immune checkpoints was significantly increased in high-risk patients. In particular, the expression of molecules, such as CD70 (CD70), cytotoxic T lymphocyte-associated protein 4 (CTLA4), and PDCD1, were significantly elevated in the high-risk group (Fig. 9g). These results suggest that the immune microenvironment in high-risk groups may be suppressed by the upregulation of immunosuppressive cytokines and immune checkpoints.

2.19 Small molecule drugs

Many small molecule drugs often show drug resistance in the process of cancer treatment, resulting in poor drug efficacy, leading to renal clear cell carcinoma and worse clinical prognosis. To validate the use of drugs in different risk groups, we compared the median maximum inhibitory concentration (IC50), which can help quantify the therapeutic ability of drugs to induce cancer cell apoptosis, which is inversely proportional to the sensitivity of small molecule drugs. Using the pRRophetic algorithm, we calculated the chemotherapy effect of 12 common small molecule drugs (sunitinib, pyrimidine, paclitaxel, lenalidomide, imatinib, gemcitabine, gefitinib, erlotinib, cytarabine, cisplatin, and bosutinib) on KIRC patients to evaluate the relationship between risk score and small molecule drug resistance based on IC50. As shown in Fig. 10, the IC50 for gemcitabine, gefitinib, imatinib, and cisplatin ($P < 0.001$) was significantly higher in the high-risk group than in the low-risk group, suggesting that high-risk patients may not benefit from these drugs. Sunitinib, pyrimidine, paclitaxel, lenalidomide, erlotinib, cytarabine, and bosutinib were significantly reduced in the high-risk group, indicating that these small molecule drugs may be more sensitive and have a greater impact on high-risk patients. These results indicate that the risk prognostic model could not only classify individuals into different risk groups, but also assist in the selection of small molecule drugs according to the corresponding sensitivity values of clinically observed KIRC patients.

3 Discussion

Clear cell renal cell carcinoma (KIRC) is the most common primary malignant tumor of adult renal carcinoma, affecting over 400,000 people worldwide each year[43]. Due to early clinical symptoms being

difficult to identify, KIRC is typically diagnosed at the later stages of disease[43]. Previous studies have reported that KIRC is a hypermetabolic disease and that fetal tumors may underlie the development of renal cancer-related deaths[44]. TNM staging is a classic method for predicting KIRC prognosis based on clinical information; however, TNM staging does not take into account any genetic characteristics. Therefore, to provide personalized treatment, it is important to identify genetic characteristics and construct prognostic models to screen patients with different risks and outcomes.

In recent years, several studies have shown that immunotherapy can benefit patients with KIRC[45]. A number of published studies have described the role of immune cells in the host defense against cancer and infection[46]. There have also been studies on kidney cancer[47] immune-related characteristics involving a large number of specific cell types [48]. Immunity has proved to play a key role in the proliferation, differentiation, invasion, and metastasis of renal tumors through different pathways of tumor progression and pathogenesis[49–51].

Ferropotosis is also closely related to the prognosis of KIRC. Research has found that KIRC is sensitive to ferropotosis, and many studies have suggested the targeted activation of ferropotosis as a potential treatment for KIRC[52, 53]. In recent years, several studies have reported that the regulation of ferropotosis-related genes can influence the course and prognosis of KIRC[54].

The roles of immunity and ferropotosis in tumors are also very similar[30, 31]. Recently, studies have shown that ferropotosis exhibits crosstalk with radiation therapy and the immune system, coupled with the metabolic vulnerability of tumor cells and sensitivity differences caused by different cell states[55–57]. Many studies on the relationship between ferropotosis and immunity have provided new insights into the pathogenesis of cancer[34, 58], which can effectively improve immunosuppression[33, 59]. Our research group recently learned that immune ferropotosis-related genes are closely associated with cancer, and their expression levels vary at different cancer stages. However, few studies have linked the prognosis and treatment of KIRC to ferropotosis-related genes, and we hope to illustrate this correlation through our analysis.

In this study, we performed a Venn diagram analysis based on the differential gene of renal clear cell carcinoma and the gene associated with immune ferropotosis in TCGA. We obtained 103 co-expressed immunoiron-mortality associated DEGs and established prognostic risk models following Lasso-Cox regression analysis to gain insights into the pathogenesis of KIRC, as well as establishing an effective tool for predicting treatment outcomes of KIRC with the aim of improving the treatment and prognosis of this disease. We also screened four immune-ferropotosis-related genes from 52 immune-ferropotosis-related prognostic genes and effectively divided KIRC patients into high- and low-risk groups based on the median risk score. Risk score is the dominant factor in prognostic risk models and rologrames. Our results were well correlated with clinical outcomes, suggesting that the model is a good predictive risk factor.

By conducting high-low risk differential analysis and GO enrichment analysis, we found that risk differential genes were not only involved in complement activation (classical approach) and the complement activation of circulating immunoglobulin mediated humoral immune response, but also in

antigen binding, immunoglobulin receptor binding, and chemokine activity, among other functions. The activity of chemokines plays an important role in the development and differentiation of immune cells in the immune microenvironment. At the same time, we performed GSEA analysis, which found enrichment in diseases, immune system, innate immune system, hemostasis, and infectious diseases. These findings confirm the role of differential genes in the development and progression of KIRC and validate the correlation of prognostic models with KIRC immune regulation.

Genes, such as CCDC134, play an important role in tumor progression[60]. Among these, STEAP1[61] is expected to be a potential target for predicting the prognosis of different types of cancer. We further evaluated the expression of four prognostic genes by protein, subcellular localization, and single-cell analysis. As a result, the mRNA and protein expression levels of LURAP1L and PLA2G6 in renal carcinoma were found to be significantly higher than those in normal tissues, while the expression levels of ACADSB and CHAC1 were significantly lower than those in normal tissues. In subcellular localization analysis, ACADSB and CHAC1 were found to be mainly distributed in the mitochondria of U-2OS cells, while LURAP1L was mainly distributed in the nucleoli of A-431 cells. PLA2G6 was mainly distributed in the cytoplasm of the central line satellite of U-2OS cells. This provides a basis for subsequent research on the corresponding mechanism of action.

In the tumor microenvironment, cancer cells and immune cells exert a large number of chemokines and cytokines to regulate the pathogenesis and progression of tumor. In this study, we found a particularly significant increase in regulatory T cells. The powerful immunosuppressive microenvironment in cancer is a key challenge for cancer therapy. Tregs and tumor-associated macrophages can directly reduce the activity of T cells in the immune microenvironment, resulting in suppression of immune function. It can also affect the aggressiveness of tumors by affecting lactic acid metabolism. In this study, immune infiltration analysis found an increase in the number of infiltrating immune cells, such as CD8 + T in the high-risk group. However, this grouping was positively correlated with PD-1 expression. Therefore, although this gene can recruit immune cells into tumor tissue, the high expression of PD-1 inactivates T cells. Therefore, the high-risk group continued to exhibit an inhibitory effect on tumor immune response.

SsGSEA showed higher immune function in the high-risk group in terms of immune checkpoint, cytolysis activity, proinflammatory, T cell co-inhibition, and type II interferon response. Significant differences were observed among the different risk groups of KIRC patients. The combination of ferropotosis and ICI can synergistically promote antitumor activity, even in ICI resistance[62]. Due to the importance of checkpoint inhibitor-based immunotherapy, our data showed significant differences in the expression of immune checkpoint-related genes between the two groups of KIRC patients, highlighting the potential significance of IFRSig in regulating ICI.

Some studies have confirmed that the TIDE algorithm can be used as a predictive model for immunotherapy[63]. The immune avoidance mechanisms adapted to renal clear cell carcinoma include the downregulation of antigen presentation or recognition, a lack of immune effector cells, the obstruction of anti-tumor immune cell maturation, an accumulation of immunosuppressive cells, the production of

inhibitory cytokines, chemokines, or ligands/receptors, and the upregulation of immune checkpoint modulators. Together with altered metabolism and hypoxia conditions, these constitute the tumor microenvironment, suggesting that IFRSig in KIRC patients may be involved in immune escape.

Antibodies based on immune checkpoint inhibitors have been reported to improve survival in patients with a variety of cancers, including lung cancer, malignant melanoma, and bladder cancer[64]. High levels of CD80 help maintain tolerance and immunosuppression in epithelial ovarian cancer[65]. The tumor microenvironment induces CTLA4 + regulatory T cell migration through CC-motif chemokine ligand 22 (CCL22) and CC-motif chemokine receptor 4 (CCR4)[66, 67]. CTLA4 immunotherapy in tumors[68] has shown good anticancer effects. Pd-l1 interacts with the corresponding receptors to inhibit the anti-tumor activity of immune cells and enable cancer cells to evade immune surveillance[69]. Drug-resistant tumor cells show an inhibition of immune-stimulating molecules and an increased expression of CD274[70]. In this study, we further evaluated the expression levels of these immunosuppressive checkpoint inhibitors and found significant differences in CTLA4, PDCD1, CD276, CD70, and other immune checkpoints in the high- and low-risk groups. In particular, both CTLA4 and CD274 were upregulated in the high-risk group, suggesting that these immune checkpoints play an important immunosuppressive role in KIRC.

Finally, the differences observed in the survival time of KIRC patients in the high- and low-risk groups may also be due to their different sensitivities to chemotherapy drugs. Patients with clear cell carcinoma of the kidney usually survive longer after receiving drug chemotherapy, while patients who are insensitive to chemotherapy drugs should receive an alternative treatment in a timely manner. To improve the prognosis of patients, as well as in response to the fact that a lack of response to drugs has implications on clinical decision making, we analyzed the chemotherapy drug resistance and sensitivity, as well as small drug molecules, to predict IFRSig potential to determine the efficacy of treatment.

Based on the four genes analyzed, diagnostic and prognostic kits for KIRC can be developed that provide potential comprehensive targets for future therapeutic interventions of KIRC. We believe that in the future, more prominent translational and clinical studies will be able to confirm the results observed in our work. Although our results provide new insights into the underlying mechanisms of immune ferropotosis that can predict the prognosis of KIRC, several limitations remain and further study is required. First, only samples from the TCGA cohort were used to build our model, and it will be necessary to use different groups and databases, such as the GEO database or multi-center cohort, to verify the accuracy of this model. Second, traceability data from a common database was used to build and validate the model. Prospective data to evaluate the clinical efficacy of KIRC are limited, and its molecular mechanism has not been determined. Therefore, further experiments and clinical data will be needed to validate the interaction between renal clear cell carcinoma and the expression of immune-ferropotosis genes.

4 Conclusion

In this study, genes associated with immune ferropotosis with independent prognostic value were identified through comprehensive bioinformatics analysis and used to establish a prognostic risk model.

Significant correlations were observed between immune ferropotosis related genes and immune score, immune checkpoint, and small molecule drugs. From this, IFRSig was found to be an independent prognostic feature that may be able to estimate OS and clinical treatment response in patients with KIRC. Furthermore, ACADSB, CHAC1, LURAP1L, and PLA2G6 were identified as potential targets and effective prognostic biomarkers of immune-combined ferropotosis. Therefore, this study provides new perspectives on the role of immune ferropotosis genes in the development of KIRC. Taken together, the model developed in this study, IFRSig, is closely related to the prognosis of KIRC and can be used to better estimate OS and predict patient responses to the clinical treatment combined with immunological characteristics.

5 Materials And Methods

5.1 Resources

5.1.1 The Cancer Genome Atlas (TCGA)

The TCGA database (https://portal.gdc.cancer.gov/) was used to download and open renal clear cell carcinoma in patients with clinical data and gene transcription. The RNA-seq and clinical data of 539 patients with renal clear cell carcinoma in the HT-SEQ-FPKM dataset were included in this study after excluding nine patients without clinical follow-up information. The clinical data included the extraction of clinical data with Perl software, where the row name was the gene name and the column name contained the matrix of KIRC patients' age, sex, survival time, survival status, grade, stage, and TNM stage information. RNA-seq raw data were normalized in UNITS per million transcripts (TPM) for subsequent analysis. TPM was used as an expression measure because it is considered to be more comparable between samples than FPKM and transcripts per million mapped readings. After extracting the transcribed data with Perl, the matrix under the ensembleID and the row name as the sample name was obtained. ID transformation was performed to obtain the matrix including sample name, gene name, and gene expression level information. The TCGA cohort information is summarized in Table 1.

5.1.2 Acquisition of genes related to immunity and ferropotosis

By integrating data from the literature[35], as well as ferropotosis databases (the FerrDb database (http://www.datjar.com:40013/bt2104/#); ferropotosis genes in the database included three types of tumor promoting, inhibition and markers) and immune-related databases (genes data from the ImmPort database (https://immport.org/shared/home) and GeneCards database (www.genecards.org)), 398 genes related to ferropotosis and 17,500 genes related to immune-related gene sets were obtained.

5.2 Research design

The datasets used in this study are all accessible and downloadable by TCGA. Based on the genomic data of TCGA, a prognostic model of immune ferropotosis risk was established for four genes. Based on

the median risk score, the samples were divided into high- and low-risk groups, and the clinical characteristics, immune microenvironment, drug treatment response, and prognosis between the two groups were subsequently analyzed.

5.3 Determination of differentially expressed genes related to the prognosis of immune ferropotosis

The “limma” package in R was used to determine the TCGA differentially expressed genes (DEGs) between tumor tissues and normal tissues (false discovery rate (FDR) < 0.05 and |log2 fold-change (FC) | > 1). Screening genes (IFR-DEG) that overlapped with immunity and ferropotosis by univariate Cox analysis, ifR-DEG, and prognostic genes were intersected to obtain ifR-DEGs associated with the prognosis of ferropotosis.

5.4 Prognostic model construction and validation

Lasso-Cox regression analysis was used to identify the genes used to construct the model. Using survival and GLMNET (a software package that fits generalized linear and similar models by penalty maximum likelihood fit), the regularization path computes the lasso or elastic net penalty on the value (on a logarithmic scale) of the regularization parameter lambda. The algorithm is very fast and can take advantage of sparsity in the input matrix X. It is suitable for linear, logistic and polynomial, Poisson, and Cox regression models. Multi-response linear regression, customized generalized linear model, and relaxation lasso regression model can also be fitted. The best value of the penalty coefficient λ was selected and the genes included in the model were determined by running the 10-fold cross validation possibility 1,000 times. The prognosis model of renal clear cell carcinoma was established according to the following conditions: risk score = ∑(Expi × β I), where “Exp” is model gene expression level and β is the model gene coefficient. The model was constructed by dividing the median risk score of patients with renal clear cell carcinoma from the TCGA database. All patients with renal clear cell carcinoma were classified as high-risk or low-risk, and KIRC in TCGA was randomly divided into training and verification sets at a ratio of 1:1.

5.5 PCA and t-SNE analysis

Principal component analysis (PCA) and T-distributed stochastic neighbor embedding (t-SNE) were applied to the high- and low-risk groups, respectively, according to the risk prognosis model. t-SNE for dimensionality reduction, which is convenient for visualization, was used to demonstrate the model’s ability to visually distinguish samples.

5.6 Prognostic model evaluation and survival analysis

By using the formula to derive the median value of the risk score, enrolled KIRC patients could be divided into high- and low-risk groups. Kaplan-Meier curves of the two risk groups were drawn using the “survival” package in R software. Risk score distribution, risk status, and risk heat map were used to evaluate the risk of predictive models. The receiver operating characteristic (ROC) curve of 1-year, 3-year, and 5-year overall survival (OS) rate of KIRC patients was drawn using the “survival” and “survival ROC” packages in

R.[36] The area under the curve (AUC) values of 1-year, 3-year, and 5-year overall survival were also calculated to evaluate the sensitivity and specificity of the model. In addition, univariate and multivariate Cox regression analyses were performed on the prognostic models in combination with clinical information, such as age, sex, T, N, and M pathological stages, to verify whether the model scores could be independent predictors.

5.7 Construction and evaluation of the line chart

The independent prognostic factors identified were comprehensively analyzed using the RMS package in R [37], as well as for the estimation of the 1-, 3-, and 5-year survival of KIRC patients. The calibration curve of the line graph was plotted using the nomogramEx software package to evaluate the agreement between the predicted and observed values.

5.8 Enrichment analysis of functional pathways

According to the high- and low-risk groups between DEGs ($|\log2FC| \geq 1$, FDR < 0.05), the “clusterProfiler” package in R[38], Gene Ontology (GO), Kyoto Encyclopedia of Genes and Genomes, KEGG Enrichment Analysis (FDR < 0.05), and Gene Set Enrichment Analysis (GSEA) were used[38].

5.9 Protein level verification and immunofluorescence localization

Immunohistochemical images were based on TCGA database and Human Protein Atlas (HPA) database[38], The protein expression profiles of the Clinical Proteomic Tumor Analysis Consortium (CPTAC) were used to detect prognostic model genes at cellular level by immunofluorescence localization and protein level verification.

5.10 ACADSB RNA sequencing expression measured at the single-cell level

To evaluate the expression of ferropotosis marker genes in different cell types, we obtained single-cell sequencing data from the PanglaoDB database, a user-friendly single-cell sequencing database that allows users to query and explore cell types, genetic pathways, and community-engineered markers based on single-cell clusters[39]. We applied the “sample” module to retrieve the data set in PanglaoDB. Renal tissue was selected (SRA640325;SRS2769051) for single-cell analysis.

5.11 cBioPortal

CBioPortal is a comprehensive database for KIRC (http://www.cbioportal.org/) gene mutation analysis, including amplification, mutations, and copy number variation. It also provides an overview of multi-gene genetic changes, visualization, and analysis of multi-dimensional cancer genomic data. Data is based on TCGA database. $P < 0.05$ was considered statistically significant.

5.12 Correlation analysis between risk score and tumor immune microenvironment

Infiltrating stromal cells and immune cells are important components of tumor tissue cells and play an important role in cancer biology. In this part of the study, two bioinformatics algorithms were used to assess immune cell infiltration in renal clear cell carcinoma tissues based on transcriptome sequencing data. Normalized enrichment score (NES) was used to quantify the relative abundance of each immune cell type in the tumor microenvironment of a single sample[40]. The algorithm can identify specific gene signals associated with stromal and immune cell infiltration in tumor tissues, predict the level of stromal and immune cell infiltration, and infer tumor purity by calculating stromal and immune scores through single-sample gene set enrichment analysis (ssGSEA).

The CIBERSORT algorithm is another common tumor immune microenvironment analysis method (https://cibersort.stanford.edu/about.php)[41]. This algorithm uses linear support vector regression (SVR) to select genes from the feature matrix for deconvolution and can accurately quantify the relative levels of different immune cell types based on gene transcriptome data.

5.13 Immunotherapy and drug reactivity

The tumor immune dysfunction and exclusion (TIDE) tool (http://tide.dfci.harvard.edu/) was used to calculate the TIDE score for every tumor sample as a substitution parameter that predicted the immune response to treatment. Thereafter, the R package “pRRophetic” was applied[42] (version 0.5), depending on the drug sensitivity of cancer genomics (GDSC, https://www.cancerrxgene.org/), through ridge regression and 10-fold cross-validation estimation half inhibitory concentration (IC50) of each sample for drug sensitivity prediction. Differences in drug sensitivity between the high- and low-risk groups were subsequently assessed using the Wilcoxon rank-sum test between the two groups, including cisplatin, etoposide, docetaxel, gefitinib, erlotinib, gemcitabine, and paclitaxel.

5.14 Statistical analysis

Statistical analysis was performed using R (version 3.6.3). Differences between subgroups were analyzed using the Mann–Whitney test, and P-values were corrected by the Benjamini and Hochberg methods to obtain the FDR. The survival difference between the two groups was analyzed by Kaplan-Meier curve and log-rank test. Gene correlation was analyzed using Pearson’s correlation coefficient test. Spearman correlation coefficient test was used to analyze the correlation between risk score and immune cells and immune regulatory genes. Univariate and multivariate Cox regression analyses were performed to determine the model’s risk score as an independent prognostic factor. A P-value less than 0.05 was considered statistically significant.

Abbreviations

KIRC:Kidney renal clear cell carcinoma;PD-1:Programmed Cell Death-1;ROS:Reactive Oxygen Species;ICI:Immune Checkpoint Inhibitors;PD-L1:Programmed Cell Death-Ligand 1;GSH:Glutathione;System xc-:Cystine/Glutamate Antiporter;GPX4:Glutathione Peroxidase4;TCGA:The Cancer Genome Atlas;ssGSEA:Single Sample Gene Set Enrichment Analysis;GO:Gene

Ontology;KEGG:Kyoto Encyclopedia of Genes and Genomes;TIDE:Tumor Immune Dysfunction and Exclusion;HPA:Human Protein Atlas;Tregs:regulatory T cells;ccRCC:Clear cell renal cell carcinoma;SLC7A11:Solute Carrier Family 7, Member 11;FTH1:ferritin heavy chain 1;DEGs:Differentially Expressed Genes;PCA:Principal Component Analysis;t-SNE:t-distributed stochastic neighbor embedding;ROC:receiver operating characteristic;AUC:area under the curve;

Declarations

Ethical Approval and Consent to participate

Not necessary.

Consent for publication

Not applicable.

Availability of data and materials

The raw data of this study are derived from ImmPort database (https://immport.niaid.nih.gov) ,Ferropotosis databases (http://www.datjar.com:40013/bt2104/#),TCGA database (https://portal.gdc.cancer.gov/) ,GeneCards database (www.genecards.org),HPA database(https://www.proteinatlas.org/),PanglaoDB database (https://panglaodb.se/) and CBioPortal database (http://www.cbioportal.org/), which are publicly available databases.

Competing interests

The authors declare that they have no conflicts of interest with the contents of this article.

Funding

This study was supported by Fujian Province Medical Innovation Foundation (2019-CXB-4, 2021-CXB001), Fujian Province Natural Science Key Fund Project (2021J02053, 2021J01704), Joint Funds for the innovation of science and Technology of Fujian province（2020Y9039）and Special funds for education and scientific research in Fujian Province (No. [2021]848 #), China.

Authors' contributions

L-HY, L-ZX, Z-JH, H-HP and MW performed the data collection. L-HY, L-ZX and Z-JH performed the data analysis and interpretation of results. L-HY, Q-YW, TL and PYZ wrote the original draft. J-BW and Y-BZ reviewed and provided critical comments on the manuscript. JWL and L-FY designed the study.

Acknowledgements

The authors gratefully acknowledge ImmPort database ,Ferropotosis databases,TCGA database ,GeneCards database,HPA database,PanglaoDB database and CBioPortal database, which made the data

available.

References

1. Reustle A, Di Marco M, Meyerhoff C, Nelde A, Walz JS, Winter S, Kandabarau S, Buttner F, Haag M, Backert L *et al*: **Integrative -omics and HLA-ligandomics analysis to identify novel drug targets for ccRCC immunotherapy**. Genome Med 2020, **12**(1):32.
2. Ricketts CJ, De Cubas AA, Fan H, Smith CC, Lang M, Reznik E, Bowlby R, Gibb EA, Akbani R, Beroukhim R *et al*: **The Cancer Genome Atlas Comprehensive Molecular Characterization of Renal Cell Carcinoma**. Cell Rep 2018, **23**(12):3698.
3. Yin L, Li W, Xu A, Shi H, Wang K, Yang H, Wang R, Peng B: **SH3BGRL2 inhibits growth and metastasis in clear cell renal cell carcinoma via activating hippo/TEAD1-Twist1 pathway**. EBioMedicine 2020, **51**:102596.
4. Ljungberg B, Bensalah K, Canfield S, Dabestani S, Hofmann F, Hora M, Kuczyk MA, Lam T, Marconi L, Merseburger AS *et al*: **EAU guidelines on renal cell carcinoma: 2014 update**. Eur Urol 2015, **67**(5):913–924.
5. Moch H, Cubilla AL, Humphrey PA, Reuter VE, Ulbright TM: **The 2016 WHO Classification of Tumours of the Urinary System and Male Genital Organs-Part A: Renal, Penile, and Testicular Tumours**. Eur Urol 2016, **70**(1):93–105.
6. Gupta K, Miller JD, Li JZ, Russell MW, Charbonneau C: **Epidemiologic and socioeconomic burden of metastatic renal cell carcinoma (mRCC): a literature review**. Cancer Treat Rev 2008, **34**(3):193–205.
7. Zhou J, Wang J, Hong B, Ma K, Xie H, Li L, Zhang K, Zhou B, Cai L, Gong K: **Gene signatures and prognostic values of m6A regulators in clear cell renal cell carcinoma - a retrospective study using TCGA database**. Aging (Albany NY) 2019, **11**(6):1633–1647.
8. Hanahan D, Weinberg RA: **Hallmarks of cancer: the next generation**. Cell 2011, **144**(5):646–674.
9. Cooper LA, Gutman DA, Chisolm C, Appin C, Kong J, Rong Y, Kurc T, Van Meir EG, Saltz JH, Moreno CS *et al*: **The tumor microenvironment strongly impacts master transcriptional regulators and gene expression class of glioblastoma**. Am J Pathol 2012, **180**(5):2108–2119.
10. Sima P, Vannucci L, Vetvicka V: **Immunity in cancer and atherosclerosis**. Ann Transl Med 2019, **7**(9):204.
11. Komohara Y, Hasita H, Ohnishi K, Fujiwara Y, Suzu S, Eto M, Takeya M: **Macrophage infiltration and its prognostic relevance in clear cell renal cell carcinoma**. Cancer Sci 2011, **102**(7):1424–1431.
12. Chan TA, Yarchoan M, Jaffee E, Swanton C, Quezada SA, Stenzinger A, Peters S: **Development of tumor mutation burden as an immunotherapy biomarker: utility for the oncology clinic**. Ann Oncol 2019, **30**(1):44–56.
13. Aoun F, Rassy EE, Assi T, Albisinni S, Katan J: **Advances in urothelial bladder cancer immunotherapy, dawn of a new age of treatment**. Immunotherapy 2017, **9**(5):451–460.

14. Vuong L, Kotecha RR, Voss MH, Hakimi AA: **Tumor Microenvironment Dynamics in Clear-Cell Renal Cell Carcinoma**. Cancer Discov 2019, **9**(10):1349–1357.
15. Refolo MG, Lotesoriere C, Messa C, Caruso MG, D'Alessandro R: **Integrated immune gene expression signature and molecular classification in gastric cancer: New insights**. J Leukoc Biol 2020, **108**(2):633–646.
16. Senbabaoglu Y, Gejman RS, Winer AG, Liu M, Van Allen EM, de Velasco G, Miao D, Ostrovnaya I, Drill E, Luna A *et al*: **Tumor immune microenvironment characterization in clear cell renal cell carcinoma identifies prognostic and immunotherapeutically relevant messenger RNA signatures**. Genome Biol 2016, **17**(1):231.
17. Escudier B: **Emerging immunotherapies for renal cell carcinoma**. Ann Oncol 2012, **23 Suppl 8**:viii35-40.
18. Porter R, Matulonis UA: **Immunotherapy for ovarian cancer**. Clin Adv Hematol Oncol 2022, **20**(4):240–253.
19. Rosenbaum E, Antonescu CR, Smith S, Bradic M, Kashani D, Richards AL, Donoghue M, Kelly CM, Nacev B, Chan JE *et al*: **Clinical, genomic, and transcriptomic correlates of response to immune checkpoint blockade-based therapy in a cohort of patients with angiosarcoma treated at a single center**. J Immunother Cancer 2022, **10**(4).
20. Wolf Y, Samuels Y: **Intratumor heterogeneity and anti-tumor immunity shape one another bidirectionally**. Clin Cancer Res 2022.
21. Xiong X, Chen S, Shen J, You H, Yang H, Yan C, Fang Z, Zhang J, Cai X, Dong X *et al*: **Cannabis suppresses antitumor immunity by inhibiting JAK/STAT signaling in T cells through CNR2**. Signal Transduct Target Ther 2022, **7**(1):99.
22. Angulo JC, Shapiro O: **The Changing Therapeutic Landscape of Metastatic Renal Cancer**. Cancers (Basel) 2019, **11**(9).
23. Hirschhorn T, Stockwell BR: **The development of the concept of ferroptosis**. Free Radic Biol Med 2019, **133**:130–143.
24. Liu L, Liu R, Liu Y, Li G, Chen Q, Liu X, Ma S: **Cystine-glutamate antiporter xCT as a therapeutic target for cancer**. Cell Biochem Funct 2021, **39**(2):174–179.
25. Dixon SJ, Lemberg KM, Lamprecht MR, Skouta R, Zaitsev EM, Gleason CE, Patel DN, Bauer AJ, Cantley AM, Yang WS *et al*: **Ferroptosis: an iron-dependent form of nonapoptotic cell death**. Cell 2012, **149**(5):1060–1072.
26. Koppula P, Zhuang L, Gan B: **Cystine transporter SLC7A11/xCT in cancer: ferroptosis, nutrient dependency, and cancer therapy**. Protein Cell 2021, **12**(8):599–620.
27. Zhang Y, Kong Y, Ma Y, Ni S, Wikerholmen T, Xi K, Zhao F, Zhao Z, Wang J, Huang B *et al*: **Loss of COPZ1 induces NCOA4 mediated autophagy and ferroptosis in glioblastoma cell lines**. Oncogene 2021, **40**(8):1425–1439.
28. Fang Y, Chen X, Tan Q, Zhou H, Xu J, Gu Q: **Inhibiting Ferroptosis through Disrupting the NCOA4-FTH1 Interaction: A New Mechanism of Action**. ACS Cent Sci 2021, **7**(6):980–989.

29. Tsai Y, Xia C, Sun Z: **The Inhibitory Effect of 6-Gingerol on Ubiquitin-Specific Peptidase 14 Enhances Autophagy-Dependent Ferroptosis and Anti-Tumor in vivo and in vitro**. Front Pharmacol 2020, **11**:598555.
30. Jiang X, Stockwell BR, Conrad M: **Ferroptosis: mechanisms, biology and role in disease**. Nat Rev Mol Cell Biol 2021, **22**(4):266–282.
31. Xu H, Ye D, Ren M, Zhang H, Bi F: **Ferroptosis in the tumor microenvironment: perspectives for immunotherapy**. Trends Mol Med 2021, **27**(9):856–867.
32. Schnetz M, Meier JK, Rehwald C, Mertens C, Urbschat A, Tomat E, Akam EA, Baer P, Roos FC, Brune B *et al*: **The Disturbed Iron Phenotype of Tumor Cells and Macrophages in Renal Cell Carcinoma Influences Tumor Growth**. Cancers (Basel) 2020, **12**(3).
33. Gao M, Monian P, Quadri N, Ramasamy R, Jiang X: **Glutaminolysis and Transferrin Regulate Ferroptosis**. Mol Cell 2015, **59**(2):298–308.
34. Sun X, Niu X, Chen R, He W, Chen D, Kang R, Tang D: **Metallothionein-1G facilitates sorafenib resistance through inhibition of ferroptosis**. Hepatology 2016, **64**(2):488–500.
35. Song Y, Tian S, Zhang P, Zhang N, Shen Y, Deng J: **Construction and Validation of a Novel Ferroptosis-Related Prognostic Model for Acute Myeloid Leukemia**. Front Genet 2021, **12**:708699.
36. Blanche P, Dartigues JF, Jacqmin-Gadda H: **Estimating and comparing time-dependent areas under receiver operating characteristic curves for censored event times with competing risks**. Stat Med 2013, **32**(30):5381–5397.
37. Liu J, Lichtenberg T, Hoadley KA, Poisson LM, Lazar AJ, Cherniack AD, Kovatich AJ, Benz CC, Levine DA, Lee AV *et al*: **An Integrated TCGA Pan-Cancer Clinical Data Resource to Drive High-Quality Survival Outcome Analytics**. Cell 2018, **173**(2):400–416 e411.
38. Yu G, Wang LG, Han Y, He QY: **clusterProfiler: an R package for comparing biological themes among gene clusters**. OMICS 2012, **16**(5):284–287.
39. Franzen O, Gan LM, Bjorkegren JLM: **PanglaoDB**: **a web server for exploration of mouse and human single-cell RNA sequencing data**. *Database (Oxford)* 2019, **2019**.
40. Yoshihara K, Shahmoradgoli M, Martinez E, Vegesna R, Kim H, Torres-Garcia W, Trevino V, Shen H, Laird PW, Levine DA *et al*: **Inferring tumour purity and stromal and immune cell admixture from expression data**. Nat Commun 2013, **4**:2612.
41. Newman AM, Liu CL, Green MR, Gentles AJ, Feng W, Xu Y, Hoang CD, Diehn M, Alizadeh AA: **Robust enumeration of cell subsets from tissue expression profiles**. Nat Methods 2015, **12**(5):453–457.
42. Geeleher P, Cox N, Huang RS: **pRRophetic: an R package for prediction of clinical chemotherapeutic response from tumor gene expression levels**. PLoS One 2014, **9**(9):e107468.
43. Bray F, Ferlay J, Soerjomataram I, Siegel RL, Torre LA, Jemal A: **Global cancer statistics 2018: GLOBOCAN estimates of incidence and mortality worldwide for 36 cancers in 185 countries**. CA Cancer J Clin 2018, **68**(6):394–424.
44. Hsieh JJ, Purdue MP, Signoretti S, Swanton C, Albiges L, Schmidinger M, Heng DY, Larkin J, Ficarra V: **Renal cell carcinoma**. Nat Rev Dis Primers 2017, **3**:17009.

45. Chevrier S, Levine JH, Zanotelli VRT, Silina K, Schulz D, Bacac M, Ries CH, Ailles L, Jewett MAS, Moch H *et al*: **An Immune Atlas of Clear Cell Renal Cell Carcinoma**. Cell 2017, **169**(4):736–749 e718.
46. Biswas SK: **Metabolic Reprogramming of Immune Cells in Cancer Progression**. Immunity 2015, **43**(3):435–449.
47. Zhang J, Yan A, Cao W, Shi H, Cao K, Liu X: **Development and validation of a VHL-associated immune prognostic signature for clear cell renal cell carcinoma**. Cancer Cell Int 2020, **20**(1):584.
48. Liu Y, Wu J, Huang W, Weng S, Wang B, Chen Y, Wang H: **Development and validation of a hypoxia-immune-based microenvironment gene signature for risk stratification in gastric cancer**. J Transl Med 2020, **18**(1):201.
49. He M, Li M, Guan Y, Wan Z, Tian J, Xu F, Zhou H, Gao M, Bi H, Chong T: **A New Prognostic Risk Score: Based on the Analysis of Autophagy-Related Genes and Renal Cell Carcinoma**. Front Genet 2021, **12**:820154.
50. Li W, Meng X, Yuan H, Xiao W, Zhang X: **A Novel Immune-Related ceRNA Network and Relative Potential Therapeutic Drug Prediction in ccRCC**. Front Genet 2021, **12**:755706.
51. Huang Y, Chen S, Xiao L, Qin W, Li L, Wang Y, Ma L, Yuan X: **A Novel Prognostic Signature for Survival Prediction and Immune Implication Based on SARS-CoV-2-Related Genes in Kidney Renal Clear Cell Carcinoma**. Front Bioeng Biotechnol 2021, **9**:744659.
52. Yang WS, SriRamaratnam R, Welsch ME, Shimada K, Skouta R, Viswanathan VS, Cheah JH, Clemons PA, Shamji AF, Clish CB *et al*: **Regulation of ferroptotic cancer cell death by GPX4**. Cell 2014, **156**(1–2):317–331.
53. Yang WH, Ding CC, Sun T, Rupprecht G, Lin CC, Hsu D, Chi JT: **The Hippo Pathway Effector TAZ Regulates Ferroptosis in Renal Cell Carcinoma**. Cell Rep 2019, **28**(10):2501–2508 e2504.
54. Mou Y, Wu J, Zhang Y, Abdihamid O, Duan C, Li B: **Low expression of ferritinophagy-related NCOA4 gene in relation to unfavorable outcome and defective immune cells infiltration in clear cell renal carcinoma**. BMC Cancer 2021, **21**(1):18.
55. Yamaguchi H, Hsu JL, Chen CT, Wang YN, Hsu MC, Chang SS, Du Y, Ko HW, Herbst R, Hung MC: **Caspase-independent cell death is involved in the negative effect of EGF receptor inhibitors on cisplatin in non-small cell lung cancer cells**. Clin Cancer Res 2013, **19**(4):845–854.
56. Lv C, Qu H, Zhu W, Xu K, Xu A, Jia B, Qing Y, Li H, Wei HJ, Zhao HY: **Low-Dose Paclitaxel Inhibits Tumor Cell Growth by Regulating Glutaminolysis in Colorectal Carcinoma Cells**. Front Pharmacol 2017, **8**:244.
57. Yang ND, Tan SH, Ng S, Shi Y, Zhou J, Tan KS, Wong WS, Shen HM: **Artesunate induces cell death in human cancer cells via enhancing lysosomal function and lysosomal degradation of ferritin**. J Biol Chem 2014, **289**(48):33425–33441.
58. Wang G, Xie L, Li B, Sang W, Yan J, Li J, Tian H, Li W, Zhang Z, Tian Y *et al*: **A nanounit strategy reverses immune suppression of exosomal PD-L1 and is associated with enhanced ferroptosis**. Nat Commun 2021, **12**(1):5733.

59. Ou Y, Wang SJ, Li D, Chu B, Gu W: **Activation of SAT1 engages polyamine metabolism with p53-mediated ferroptotic responses**. Proc Natl Acad Sci U S A 2016, **113**(44):E6806-E6812.
60. Huang Z, Yang L, Chen J, Li S, Huang J, Chen Y, Liu J, Wang H, Yu H: **CCDC134 as a Prognostic-Related Biomarker in Breast Cancer Correlating With Immune Infiltrates**. Frontiers in Oncology 2022, **12**.
61. Zhao C, Xiong K, Ji Z, Liu F, Li X: **The Prognostic Value and Immunological Role of STEAP1 in Pan-Cancer: A Result of Data-Based Analysis**. Oxid Med Cell Longev 2022, **2022**:8297011.
62. Tang R, Xu J, Zhang B, Liu J, Liang C, Hua J, Meng Q, Yu X, Shi S: **Ferroptosis, necroptosis, and pyroptosis in anticancer immunity**. J Hematol Oncol 2020, **13**(1):110.
63. Xu F, Huang X, Li Y, Chen Y, Lin L: **m(6)A-related lncRNAs are potential biomarkers for predicting prognoses and immune responses in patients with LUAD**. Mol Ther Nucleic Acids 2021, **24**:780–791.
64. Wei Y, Ou T, Lu Y, Wu G, Long Y, Pan X, Yao D: **Classification of ovarian cancer associated with BRCA1 mutations, immune checkpoints, and tumor microenvironment based on immunogenomic profiling**. PeerJ 2020, **8**:e10414.
65. Macpherson AM, Barry SC, Ricciardelli C, Oehler MK: **Epithelial Ovarian Cancer and the Immune System: Biology, Interactions, Challenges and Potential Advances for Immunotherapy**. J Clin Med 2020, **9**(9).
66. Curiel TJ, Coukos G, Zou L, Alvarez X, Cheng P, Mottram P, Evdemon-Hogan M, Conejo-Garcia JR, Zhang L, Burow M *et al*: **Specific recruitment of regulatory T cells in ovarian carcinoma fosters immune privilege and predicts reduced survival**. Nat Med 2004, **10**(9):942–949.
67. Landskron J, Helland O, Torgersen KM, Aandahl EM, Gjertsen BT, Bjorge L, Tasken K: **Activated regulatory and memory T-cells accumulate in malignant ascites from ovarian carcinoma patients**. Cancer Immunol Immunother 2015, **64**(3):337–347.
68. Wei C, Liu X, Wang Q, Li Q, Xie M: **Identification of Hypoxia Signature to Assess the Tumor Immune Microenvironment and Predict Prognosis in Patients with Ovarian Cancer**. Int J Endocrinol 2021, **2021**:4156187.
69. Chen J, Jiang CC, Jin L, Zhang XD: **Regulation of PD-L1: a novel role of pro-survival signalling in cancer**. Ann Oncol 2016, **27**(3):409–416.
70. Cacan E: **Epigenetic-mediated immune suppression of positive co-stimulatory molecules in chemoresistant ovarian cancer cells**. Cell Biol Int 2017, **41**(3):328–339.

Tables

Table 1 Baseline information of TCGA

variable	layered	TCGA
Age (%)	65 or less	348 (65.7%)
	> 65	182 (34.3%)
Gender (%)	women	189 (35.6%)
	men	341 (64.3%)
Stage (%)	Stage I	266 (50.1%)
	Stage II	56 (10.5%).
	Stage III	125 (23.5%)
	Stage IV	83 (15.6%)
Grade (%)	G1	15 (2.8 %)
	G2	229 (43.2%)
	G3	208 (39.2%)
	G4	78 (14.7%)

Table 2 Functional enrichment analysis of high and low risk groups in TCGA cohort

ONTOLOGY	ID	Description	Gene Ratio	BgRatio	p-value	p.adjust	q-value
BP	GO:0006958	complement activation, classical pathway	42/152	137/18670	7.04 e-56	1.64 e-52	1.43 e-52
BP	GO:0002455	humoral immune response mediated by circulating immunoglobulin	42/152	150/18670	5.81 e-54	6.76 e-51	5.90 e-51
BP	GO:0006956	complement activation	42/152	175/18670	8.80 e-51	6.83 e-48	5.96 e-48
BP	GO:0072376	protein activation cascade	42/152	198/18670	2.70 e-48	1.57 e-45	1.37 e-45
BP	GO:0016064	immunoglobulin mediated immune response	43/152	218/18670	5.32 e-48	2.48 e-45	2.16 e-45
CC	GO:0019814	immunoglobulin complex	50/158	159/19717	1.00 e-67	1.57 e-65	1.50 e-65
CC	GO:0042571	immunoglobulin complex, circulating	27/158	72/19717	8.58 e-39	6.73 e-37	6.41 e-37
CC	GO:0072562	blood microparticle	21/158	147/19717	1.48 e-20	7.73 e-19	7.36 e-19
CC	GO:0009897	external side of plasma membrane	29/158	393/19717	7.06 e-20	2.77 e-18	2.64 e-18
CC	GO:0034364	high-density lipoprotein particle	4/158	26/19717	5.17 e-05	0.002	0.002
MF	GO:0003823	antigen binding	42/133	160/17697	1.76 e-54	4.76 e-52	4.20 e-52
MF	GO:0034987	immunoglobulin receptor binding	26/133	76/17697	5.08 e-37	6.86 e-35	6.04 e-35
MF	GO:0008009	chemokine activity	5/133	49/17697	3.25 e-05	0.003	0.003
MF	GO:0042379	chemokine receptor binding	5/133	66/17697	1.38 e-04	0.008	0.007
MF	GO:0015926	glucosidase activity	3/133	14/17697	1.42 e-04	0.008	0.007

KEGG	hsa04061	Viral protein interaction with cytokine and cytokine receptor	8/57	100/8076	4.17 e-07	5.76 e-05	5.19 e-05
KEGG	hsa04060	Cytokine-cytokine receptor interaction	9/57	295/8076	1.97 e-04	0.010	0.009
KEGG	hsa03320	PPAR signaling pathway	5/57	78/8076	2.09 e-04	0.010	0.009
KEGG	hsa05323	Rheumatoid arthritis	5/57	93/8076	4.74 e-04	0.016	0.015
KEGG	hsa04978	Mineral absorption	4/57	59/8076	7.61 e-04	0.021	0.019

Figures

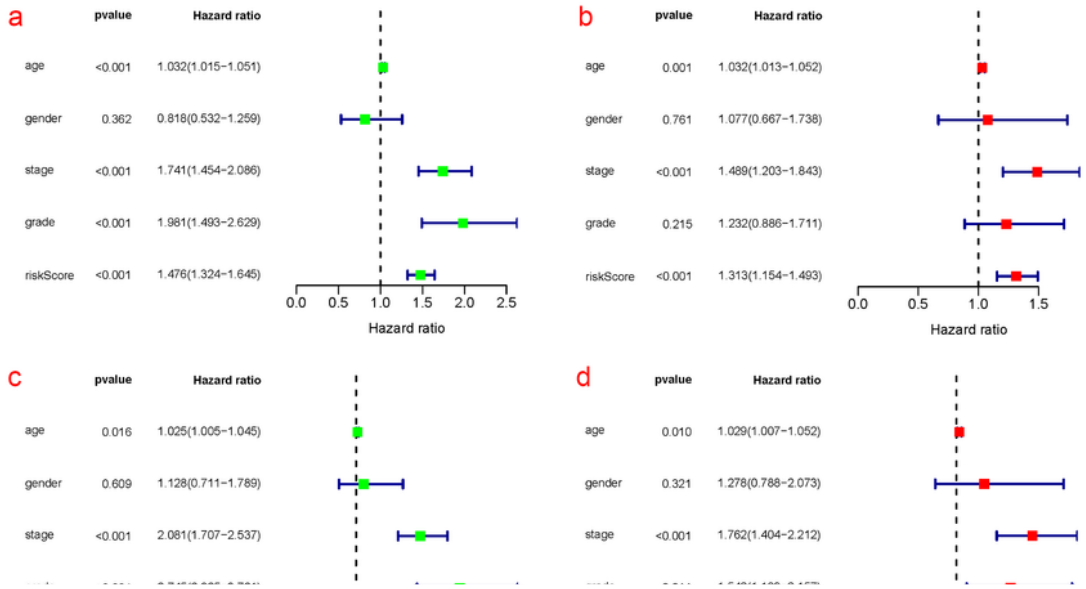

Figure 3

Univariate Cox regression analysis of prognostic index validation of genes associated with immune ferropotosis (a, c, e), Multivariate Cox regression analysis (b, d, f). training set (a, b); validation set (c, d); TCGA cohort (e, f). Construction and validation of a column diagram (g, h). (g) Survival nomogram based on the TCGA cohort. (h) Calibration curves to predict 1-, 3-, and 5-year survival for KIRC patients in the TCGA cohort.

Figure 8

(a)Correlation of different immune cells. Heat maps of correlations between 22 immune cells. Blue and red represent positive and negative correlations, respectively.(b)Relationship between risk score and immune cell infiltration and related functions analyzed by ssGSEA. The score refers to the immune score, the higher the score, the deeper the immune cell infiltration (*$P < 0.05$, **$P < 0.01$, and ***$P < 0.001$).(c-h)Immune microenvironment and prognosis. KM survival analysis showed that Treg cells, CD4+T memory cells, follicular helper T cells, monocytes, non-activated mast cells, and resting dendritic cells were significantly correlated with survival time.